Morphological changes of InGaN epilayers during annealing assessed by spectral analysis of atomic force microscopy images

Rachel A. Oliver, Joy Sumner, Menno J. Kappers, and Colin J. Humphreys

Citation: Journal of Applied Physics **106**, 054319 (2009); doi: 10.1063/1.3212971
View online: https://doi.org/10.1063/1.3212971
View Table of Contents: http://aip.scitation.org/toc/jap/106/5
Published by the American Institute of Physics

Morphological changes of InGaN epilayers during annealing assessed by spectral analysis of atomic force microscopy images

Rachel A. Oliver,[a] Joy Sumner, Menno J. Kappers, and Colin J. Humphreys
Department of Materials Science and Metallurgy, University of Cambridge, Pembroke Street, Cambridge CB2 3QZ, United Kingdom

(Received 14 May 2009; accepted 30 July 2009; published online 15 September 2009)

During annealing, the morphologies of thin InGaN epilayers have been observed to change from a terraced structure to a network of interlinking InGaN strips separated by troughs. This change in morphology may contribute to high efficiencies in some GaN-based light emitting diodes (LEDs) if the InGaN is exposed to elevated temperatures without a protective GaN capping layer. Here, we investigate the changes in morphology which occur when InGaN epilayers are annealed at their growth temperature under NH_3, N_2, and a small H_2 flux. We observe that while the layers initially roughen, more extended anneals lead to the surface becoming smooth and terraced once again. Power spectral density analysis of atomic force microscopy data is used to show that the dominant mechanism for roughening is loss of material from pre-existing pits, while the dominant smoothening mechanism is surface diffusion. This mechanistic analysis may be relevant to the growth of InGaN quantum wells in LED structures. © *2009 American Institute of Physics*. [doi:10.1063/1.3212971]

I. INTRODUCTION

Light emitting diodes (LEDs) with $In_xGa_{1-x}N$ quantum wells (QWs) in their active regions have proved enormously commercially successful. That they emit bright light, despite the presence of very high (10^8–10^{10} cm^{-2}) threading dislocation (TD) densities, was at first the cause of some amazement and remains a source of continuing scientific controversy.[1] In a previous study, we noted the existence of gross fluctuations in the width of the QWs in the active region of a commercially available green-emitting GaN-based LED.[2] To reproduce such fluctuations in a laboratory context, we observed that the $In_xGa_{1-x}N$ should be subjected to either an anneal stage at growth temperature or a ramp up to a higher temperature prior to the growth of the subsequent GaN barrier layer. Atomic force microscopy (AFM) and transmission electron microscopy (TEM) studies on analogous thin epilayers revealed that following such a growth schedule the $In_xGa_{1-x}N$ layers consisted of strips of material forming an interlinking network. Furthermore, TEM revealed that the majority of TDs intersected the sample surface in the troughs between the strips so that in a QW structure the TDs would pass through a gap in the $In_xGa_{1-x}N$ QW, i.e., through a GaN region.[2] Hence, we postulated that the network structure of the QW resulted in an increased potential barrier in the region around dislocations, preventing exciton diffusion to dislocation cores and improving optical performance.

The impact of exposure to high temperatures on thin $In_xGa_{1-x}N$ epilayers without a GaN cap has not been widely reported in the literature despite the fact that highly efficient QW structures may be realized when the $In_xGa_{1-x}N$ is exposed to a temperature ramp before the deposition of the GaN cap.[3] Most studies on the impact of annealing on $In_xGa_{1-x}N$ relate to the changes in the properties of QWs during the anneal of the *p*-type cap which is necessary during LED growth.[4] An early study on the thermal stability of the nitrides by Vartuli *et al.*[5] showed that $In_{0.5}Ga_{0.5}N$ epilayers roughened upon annealing at temperatures above 700 °C, but did not address films with the lower indium contents that are usually used in blue and green LEDs. Later, Chalker *et al.*[6] suggested that indium is lost from the surface of $In_{0.25}Ga_{0.75}N$ epilayers upon annealing at 950 °C by both inward diffusion and surface evaporation. However, both the temperature and the duration of the anneal used in this case are more severe than those which would usually be encountered during the growth of LED structures. It is only quite recently that ourselves[2] and others[7] have started to study the behavior of $In_xGa_{1-x}N$ epilayers analogous to the QWs used in LEDs under thermal treatments relevant to LED growth.

Our previous attempts to understand the formation of these network structures[8] have focused on AFM and TEM examinations of samples annealed under ammonia (NH_3) with a N_2 carrier gas. Here, we report the broader range of morphologies which may be observed when $In_xGa_{1-x}N$ epilayers are annealed under NH_3/N_2 with a small additional flux of H_2. The epilayers—which initially exhibit a terraced structure—roughen to form a network of interlinking $In_xGa_{1-x}N$ strips, as has previously been observed. However, in the presence of a H_2 flux, following more extended annealing, the roughness of the surfaces starts to decrease, and a smooth terraced structure with only a few pits reforms. By performing analysis of the power spectral density (psd) functions of the observed surface morphologies, the atomistic mechanisms involved in the smoothening and roughening processes may be assessed, potentially providing an insight into the formation of not only the particular samples described here but also $In_xGa_{1-x}N$ layers grown under other conditions which may be relevant to the inhomogeneous QWs seen in commercial devices.

[a]Electronic mail: rao28@cam.ac.uk.

II. METHODS

All samples were grown by metal-organic vapor phase epitaxy (MOVPE) on GaN pseudosubstrates in a 6×2 in. Thomas Swan close-coupled showerhead reactor. The pseudosubstrates consisted of approximately 5 μm of GaN grown on *c*-plane (0001) sapphire miscut $0.25°\pm0.10°$ toward $(11\bar{2}0)$ at 1020 °C, following deposition of a 30 nm GaN buffer at 540 °C.[9] (Temperatures quoted in this paper are the susceptor temperature measured using a pyrometer calibrated against a black body source.) The pseudosubstrates were exposed to air in order to check for macroscopic defects using optical microscopy. Hence, prior to growth of the InGaN epilayer, a 500 nm GaN connecting layer was grown to bury the regrowth interface, providing a clean, flat surface. The pseudosubstrates have a dislocation density of $(3-6)\times10^8$ cm^{-2} [as measured using AFM (Ref. 10) and TEM (Ref. 11) methods which reveal all the dislocations in the sample].

$In_xGa_{1-x}N$ was grown at a temperature of 710 °C using the precursors trimethylindium (TMI), trimethylgallium (TMG), and NH_3, with N_2 as a carrier gas at a reactor pressure of 300 Torr. The NH_3 flux was 10 slm (litres per minute at STP) as was the N_2 flux. The TMI source was maintained at 25 °C and 1000 Torr and the TMG source at 5 °C and 1500 Torr. Following growth of an approximately 3 nm thick epilayer, samples were annealed for times ranging from 0 to 960 s under the same conditions of temperature and pressure as were employed during growth. During the anneal, the NH_3 with N_2 fluxes were also identical to those employed during growth, but an additional flux of 500 SCCM (SCCM denotes cubic centimeter per minute at STP) of H_2 was introduced into the reactor. Following annealing the samples were cooled in an atmosphere of NH_3 and N_2.

The variation in sample morphology with annealing time was investigated using a Veeco Dimension 3100 AFM in intermittent contact mode. Images were then processed and analyzed using the WSXM freeware,[12] which was also used to calculate fast Fourier transforms of the data and the related psd functions. These functions were analyzed using a method based on that developed by Tong and Williams,[13] which will be described in more detail in Sec. IV. This approach has occasionally been applied to the analysis of GaN samples in the past, notably by Koleske *et al.*[14] who assessed the mechanisms of growth of GaN nuclei during the annealing of GaN nucleation layers grown on sapphire and found that evaporation of material and recondensation governed the growth process. Additionally, we have previously used a simple version of this analysis to assess the variation in lateral length scales in samples annealed in only N_2 and NH_3.[15]

III. RESULTS

Figure 1 shows the evolution in the morphology of an $In_xGa_{1-x}N$ layer as the annealing time increases from 0 to 960 s. Prior to annealing, the $In_xGa_{1-x}N$ epilayer [Fig. 1(a)] displays a terraced morphology, with nanoscale raised features decorating the edges of the terraces, as we have previously reported.[16] Following a short anneal with a H_2 flux [60 s, Fig. 1(b)], the observed morphology is rather similar to

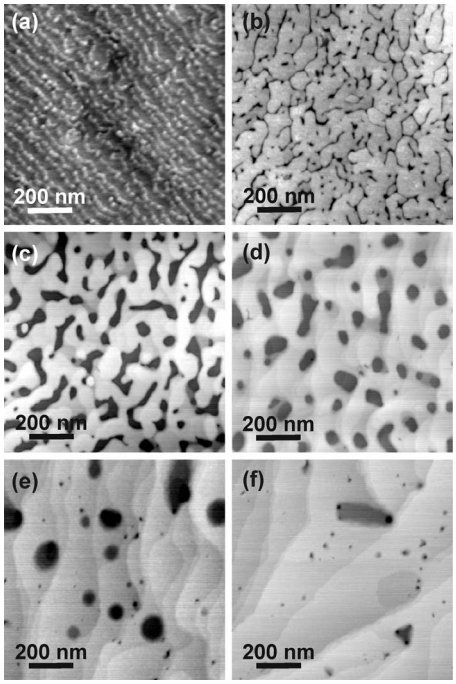

FIG. 1. AFM images of $In_xGa_{1-x}N$ epilayers which have been annealed in 10 slm of NH_3 and 10 slm of N_2 with an additional flux of 500 SCCM of H_2: (a) anneal time $t=0$ s and image height $h=1.2$ nm, (b) $t=60$ s and $h=4.9$ nm, (c) $t=240$ s and $h=6.6$ nm, (d) $t=360$ s and $h=5.7$ nm, (e) $t=480$ s and $h=4.17$ nm, and (f) $t=960$ s and $h=7.3$ nm.

that which we have previously reported[8] for longer anneal times (240–480 s) when similar $In_xGa_{1-x}N$ layers are annealed in only N_2 and NH_3. The sample exhibits narrow, elongated pits; the depth of which may be underestimated by AFM measurements since the tip may not penetrate to the bottom of the feature. For a longer anneal time (240 s) with a H_2 flux, the observed pits [Fig. 1(c)] are significantly wider. After a 360 s anneal with a H_2 flux, many of the observed pits appear more rounded and less elongated [Fig. 1(d)]. Nonetheless, the structure could still be described as a network of interlinking $In_xGa_{1-x}N$ strips separated by pits, i.e., as a variant on the morphologies we have previously observed.

However, for anneal times in excess of 360 s, our observations are perhaps more surprising and are significantly different from our previous observations[8] for annealing under just NH_3 and N_2. For a 480 s anneal [Fig. 1(e)], the number of pits per unit area appears significantly reduced compared to shorter anneal times, and for the longest anneal time examined here [960 s, Fig. 1(f)], very few wide, deep pits remain and the surface has resumed a terraced morphology albeit one in which step bunching has lead to a greater step spacing than that observed in Fig. 1(a). Although this surface appears somewhat reminiscent of the GaN pseudosubstrate surface which underlies the $In_xGa_{1-x}N$ layer, photoluminescence measurements reveal emission peaking at 422 nm, which suggests that although the indium content of the film may have decreased (since epilayers annealed for shorter times show emission peaking at longer wavelengths) there is still $In_xGa_{1-x}N$ present on the surface.

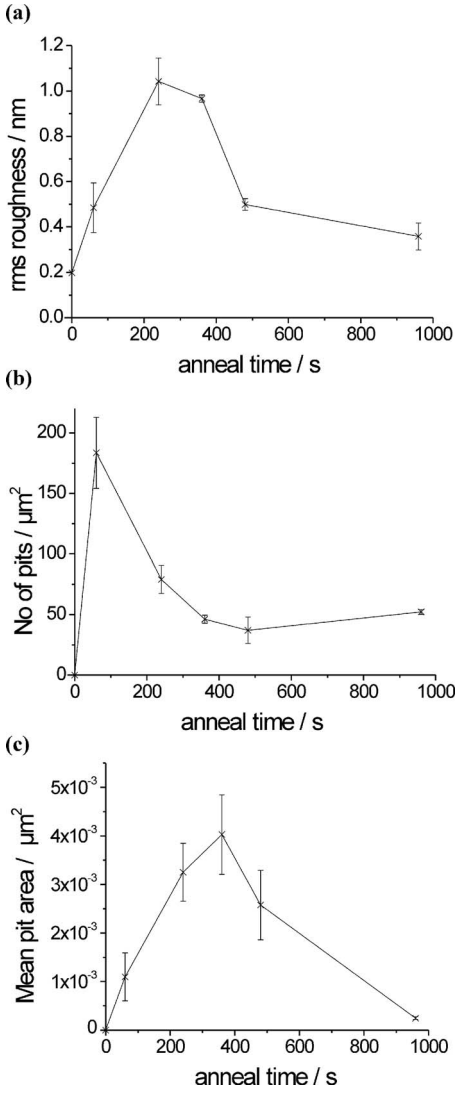

FIG. 2. Basic quantification of morphological variations seen in Fig. 1. (a) The variation in the rms roughness of the $In_xGa_{1-x}N$ surface with anneal time. (b) The variation in the number of pits found in a 1×1 μm^2 area of the $In_xGa_{1-x}N$ surface with anneal time. (c) The variation in the average area of the pits in the $In_xGa_{1-x}N$ surface with anneal time.

In order to quantify the morphological variation observed above, we display in Fig. 2(a) the variation in the root mean square (rms) roughness of the $In_xGa_{1-x}N$ surface with anneal time. The analysis was performed using data from four 3×3 μm^2 images. While the rms roughness initially increases with anneal time (as was observed for annealing without a H_2 flux[8]), it then decreases again so that following a 960 s anneal, it has returned almost to its original value prior to annealing. The origin of these variations in roughness is further quantified in Figs. 2(b) and 2(c) which illustrate the number of pits found in a 1×1 μm^2 area and the average area of those pits, respectively. These data indicate that the initial increase in roughness relates to the formation of pits and their growth, and the subsequent decrease in roughness relates to the shrinking and disappearance of pits. To analyze the observed variations in roughness in more detail we employed psd functions, as described in Sec. IV.

IV. ANALYSIS

A. Approach

While the rms roughness is a standard metric to quantify the variations in height of the surface, it is unaffected by the lateral scale of the morphological variation. To more fully quantify and understand the observed changes in morphology requires an analysis method which takes into account the full three-dimensional nature of the surface. Here, attempting to achieve this, we have employed a method initially developed by Tong and Williams[13] for the assessment of morphological development during the deposition of thin films, but which is equally applicable to the etching or decomposition of layers.[13]

In using AFM data to analyze the morphological change of the surface, we consider the data as a mathematical function $H(\boldsymbol{r},t)$, where H is the measured surface height at position vector $\boldsymbol{r}$ at time t. This differs from the absolute height of the surface $S(\boldsymbol{r},t)$ since the average height value of an AFM data set is usually zero so that $H(\boldsymbol{r},t)=S(\boldsymbol{r},t)-\langle S(\boldsymbol{r},t)\rangle$, where $\langle S(\boldsymbol{r},t)\rangle$ denotes the mean of $S(\boldsymbol{r},t)$. Tong and Williams[13] showed that it is possible to write an equation of motion for the growing surface—essentially a kinetic rate equation—in terms of $h(|\boldsymbol{q}|,t)$, the radial average of the Fourier transform of $H(\boldsymbol{r},t)$:

$$\frac{\partial h(|\boldsymbol{q}|,t)}{\partial t} \propto -c_n|q|^n h(|\boldsymbol{q}|,t)+\eta(|\boldsymbol{q}|,t). \tag{1}$$

In Eq. (1), the smoothing exponent n depends on the mechanism by which smoothing occurs, and c_n is a constant relating to that smoothing mechanism. The function $\eta(|\boldsymbol{q}|,t)$ is a stochastic noise term which describes the random arrival of growth species at the surface (or for etching/decomposition the random removal of atoms from the surface). Based on the analysis of Herring,[17] Tong and Williams[13] suggested the following four smoothing exponents and related mechanisms: $n=1$ for plastic flow, $n=2$ for evaporation and recondensation, $n=3$ for bulk diffusion, and $n=4$ for surface diffusion. A solution to Eq. (1) may be found in terms of the radially averaged psd of $H(\boldsymbol{r},t)$, $g(|\boldsymbol{q}|,t)$:

$$g(|\boldsymbol{q}|,t)=\langle|h(|\boldsymbol{q}|,t)|^2\rangle=\Omega\frac{1-\exp(-2c_n|\boldsymbol{q}|^n t)}{c_n|\boldsymbol{q}|^n}. \tag{2}$$

A schematic of the form of this function is shown in Fig. 3 as a log-log plot. This illustrates how the $\boldsymbol{q}$-dependence of the spectral density depends on the smoothening mechanism.

Equation (2) is appropriate for a surface which roughens stochastically. However, Tong and Williams[13] noted that surface growth often occurs via the formation of islands (by various mechanisms) and in this case, roughening is not stochastic. Hence, they introduced two further mechanisms into their analysis: roughening by deposition of material onto existing islands and roughening by random deposition of material onto the film surface and then diffusion of that material to existing islands. The first of these mechanisms has a smoothing exponent n of 1, and the second has $n=3$. (It should be noted that for decomposition of material, one would not consider, for example, roughening by deposition

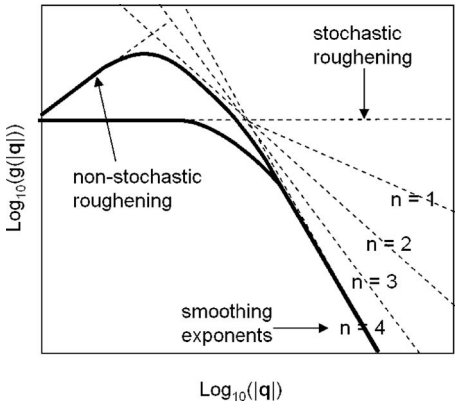

FIG. 3. Schematic diagram showing the influence of roughening and smoothing mechanisms on the psd function $g(|\boldsymbol{q}|)$.

of material onto existing islands but roughening by *loss* of material from existing *pits*). However, the signs of the constants c_n are different for roughening and smoothing. Hence, Tong and Williams rewrote Eq. (2) as follows:

$$g(|\boldsymbol{q}|,t) = \langle |h(|\boldsymbol{q}|,t)|^2 \rangle = \Omega \frac{\exp(2\Sigma \chi_n |\boldsymbol{q}|^n t) - 1}{\Sigma \chi_n |\boldsymbol{q}|^n t}. \quad (3)$$

The summation of terms in $\chi_n |\boldsymbol{q}|^n t$ indicates that for a real surface a variety of roughening and smoothening mechanisms may operate simultaneously. The constants χ_n will be positive if the exponent n relates to a net roughening mechanism and negative if n relates to a net smoothening mechanism. However, since values of n of 1 and 3 relate to both a smoothening and a roughening mechanism, a positive value of χ_3, for example, does not necessarily imply that no smoothening by bulk diffusion occurs, just that the relevant nonstochastic roughening mechanism has more effect on the surface. Hence, nonstochastic roughening mechanisms may mask the impact of smoothening by plastic flow and bulk diffusion and vice versa. The impact of the nonstochastic roughening mechanisms on the form of $g(|\boldsymbol{q}|,t)$ is shown in Fig. 3.

Having developed this formalism, Tong and Williams proceeded to fit Eq. (3) to the data for the growth of CuCl islands and studied the values of the smoothing and roughening exponents. In studying GaN growth, Koleske *et al.*[14] took a different approach. They extracted the dominant smoothing and roughening exponents by fitting a straight line to the linear portions of the log-log plot of $g(|\boldsymbol{q}|,t)$. The modulus of the gradient of this line for large $\boldsymbol{q}$—i.e., small length scales—then gives the approximate smoothing exponent while the gradient of the line at small $\boldsymbol{q}$ gives the roughening exponent. Here, we will apply both these approaches.

B. Results of analysis

Figure 4 shows log-log plots of the psd functions calculated from four 3×3 μm^2 images of the samples annealed between 60 and 480 s. For the straight line portion of the function at high values of $\boldsymbol{q}$, calculation of the gradient of the log-log plot, following the approach of Koleske *et al.*,[14] suggests smoothing exponents of approximately 4, with the measured values ranging from 3.5 to 4.5. This would be

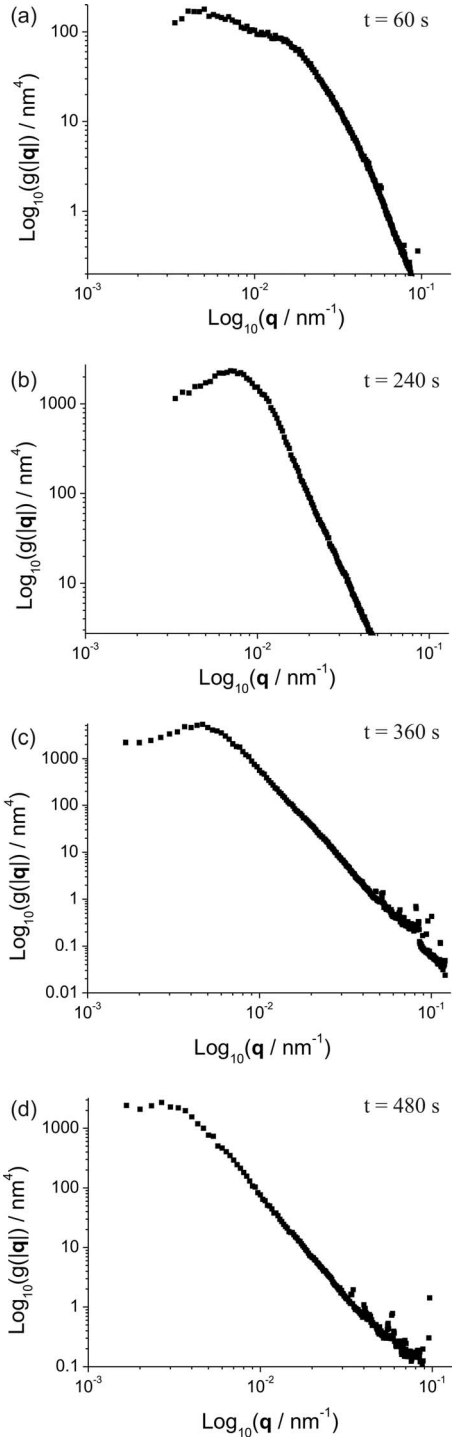

FIG. 4. psd functions calculated for 3×3 μm^2 AFM images of annealed $In_xGa_{1-x}N$ epilayers: (a) anneal time $t=60$ s, (b) $t=240$ s, (c) $t=360$ s, and (d) $t=480$ s.

consistent with smoothing occurring primarily through surface diffusion. For the samples annealed between 240 and 480 s, the portion of the psd function at low $\boldsymbol{q}$ has a positive gradient, suggesting a roughening exponent of around 1, consistent with roughening by loss of material from existing pits. The measured values for the three samples range from 1.1 to 1.3. For the sample with the shortest anneal time, the gradient of the log-log plot of the psd function is close to zero but is slightly negative (−0.4). This may imply that this sample is better modeled by stochastic roughening, suggest-

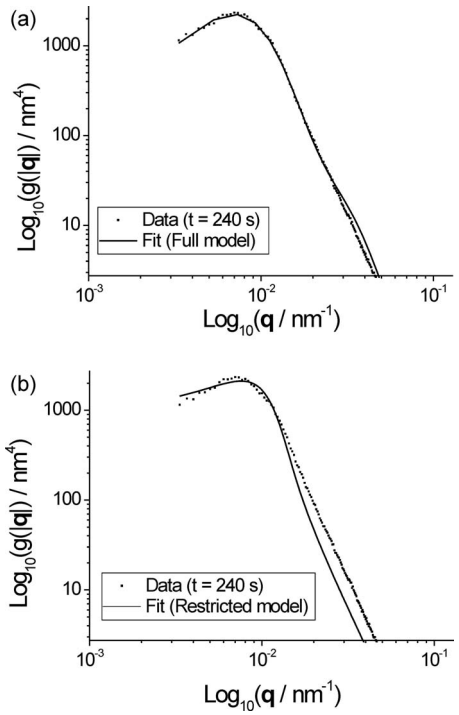

FIG. 5. Comparison of fitted and experimental psd functions calculated for the $In_xGa_{1-x}N$ epilayer annealed for 240 s. (a) Data fitted using the full function given as Eq. (3); $R^2=0.998$. (b) Data fitted using a restricted function: χ_2 and χ_3 are set to zero; $R^2=0.989$.

ing that material is lost from the surface at random positions initially. However, it should be noted that for this sample the features seen are very narrow, and given the finite size of the AFM tip it may not penetrate to the bottom of these pits. Hence, in this case the psd function may be a less reliable expression of the surface morphology than for the other samples.

To further investigate the relevance of the Tong and Williams model, we have fitted the full function given as Eq. (3) to the data shown in Fig. 4. Figure 5(a) gives an example of the fit achieved for the sample annealed for 240 s. The goodness-of-fit value R^2 for the fit shown is 0.998, indicating excellent agreement between the model and the data. The data sets shown in Fig. 4 have all been fitted to this full function, and the R^2 value is in excess of 0.99 in all cases. The fitting parameters and R^2 values are given in Table I. Looking at the table, the values of χ_1 and χ_3 are positive, indicating that they relate to net roughening mechanisms. Hence, any smoothening by plastic flow and bulk diffusion is masked by the presence of nonstochastic roughening mechanisms.

While excellent fits may be achieved using the full model, it uses a large number of parameters, and the meanings of these parameters can be difficult to interpret. Hence, based on the analysis of the psd function gradients at high and low $\boldsymbol{q}$, we have also fitted the data with a more restricted model in which the values of χ_2 and χ_3 are set to zero so that the resulting function only depends on smoothening by surface diffusion and roughening by loss of material at pre-existing pits. For the sample annealed for 60 s, where the gradient of the graph at low $\boldsymbol{q}$ suggested that roughening might occur stochastically, we have restricted the model still further by setting χ_1 to zero, hence including only stochastic roughening and smoothening by surface diffusion in our fitting function. An example of the fit achieved using the restricted model is given in Fig. 5(b) for the sample annealed for 240 s. While the fit is visibly less good in this case, the R^2 value is 0.989, suggesting that despite the reduced number of parameters used in fitting, good agreement can still be achieved. For all the restricted models used, the R^2 value is greater than 0.96. The good fits achieved with these restricted models thus support the suggestion that the main smoothening mechanism is surface diffusion and the main roughening mechanism is loss of material from pre-existing pits.

V. DISCUSSION

For either the full or the restricted model, the fitted values of the constants χ_n are seen to vary with annealing time (see Table I). A similar effect was observed by Tong and Williams for their analysis of the growth of CuCl islands, and they attributed this to the limitations of the model which does not include any possible nonlinear contributions to the equation of motion of the growing surface and may not include all the potential smoothening and roughening mechanisms. While these comments certainly apply to our samples, there may also be another effect which causes changes in the values of χ_n with annealing time: during the annealing of $In_xGa_{1-x}N$, indium is preferentially lost from the film (compared to gallium)[8] so that the overall composition of the film and chemistry of the film surface will change with time. This may alter the operation of the smoothening and roughening mechanisms and hence the values of χ_n.

While the use of the psd functions allows us to identify the likely atomic mechanisms involved in smoothening and roughening, it does not provide an explanation for why these changes occur. The formation of pits and loss of material from the pits in the annealing of $In_xGa_{1-x}N$ has been shown to result from desorption of indium-rich material, although

TABLE I. Values of the fitting coefficients when the data in Fig. 3 are fitted with Eq. (3).

Anneal time (s)	Ω	χ_1	$\chi_2/10^4$	$\chi_3/10^6$	$\chi_4/10^7$	R^2
60	69 ± 4	100 ± 20	-2.1 ± 0.2	1.1 ± 0.1	-2.2 ± 0.2	0.991
240	18 ± 1	174 ± 4	-1.79 ± 0.07	0.59 ± 0.05	-0.7 ± 0.1	0.998
360	21 ± 2	197 ± 6	-3.27 ± 0.02	1.7 ± 0.2	-3.1 ± 0.6	0.993
480	40 ± 5	130 ± 12	-3.4 ± 0.5	2.2 ± 0.7	-7 ± 2	0.993

the mechanism of formation of indium-rich regions remains controversial.[15] The degree of smoothening observed in these samples, however, has not been observed in other samples annealed without a hydrogen flux. Hence, the driving force for smoothening may relate to the presence of hydrogen. One possible reason for this is that hydrogen acts as a surfactant to the (0001) surface, hence encouraging the diffusion of material to eliminate the inclined side facets at the edges of the pits. The theoretical work by Neugebauer[18] has suggested that in MOVPE the presence of hydrogen may stabilize the (0001) surface of GaN, making this explanation plausible.

An additional limitation of this work is that only one annealing condition, in terms of temperature and pressure, has been studied. In the growth of LEDs, if a temperature ramp is employed between the deposition of the $In_xGa_{1-x}N$ and the addition of a GaN cap, the temperature will obviously vary and the pressure may also be adjusted. This may lead to changes in diffusion constants or evaporation rates so that the primary mechanisms for roughening and smoothening change during the ramp process. However, we hope that we have illustrated the usefulness of psd-based analysis for the simple set of samples described here and that similar approaches may provide further insights into the atomistic mechanisms occurring during more complex thermal treatments such as temperature ramping in the future.

VI. CONCLUSIONS

$In_xGa_{1-x}N$ films annealed in NH_3 with an additional H_2 flux initially roughen via the formation of pits, but then become smoother again at extended anneal times. A spectral analysis of the AFM data has been performed and suggests that roughening occurs nonstochastically, possibly involving the loss of material from the sidewalls of existing pits. Smoothening occurs primarily via surface diffusion. These data may give an insight into the formation of gross well-width fluctuations in green InGaN/GaN LEDs.

ACKNOWLEDGMENTS

This work has been funded, in part, by the EPSRC (Contract No. GR/S49391/01). J.S. would like to acknowledge funding from Thomas Swan Scientific Equipment Ltd. R.A.O. would like to acknowledge funding from the Royal Society.

[1] R. A. Oliver and B. Daudin, Philos. Mag. **87**, 1967 (2007).
[2] N. K. van der Laak, R. A. Oliver, M. J. Kappers, and C. J. Humphreys, Appl. Phys. Lett. **90**, 121911 (2007).
[3] M. J. Galtrey, R. A. Oliver, M. J. Kappers, C. McAleese, D. Zhu, C. J. Humphreys, P. H. Clifton, D. J. Larson, and A. Cerezo, Appl. Phys. Lett. **92**, 041904 (2008).
[4] B. Van Daele, G. Van Tendeloo, K. Jacobs, I. Moerman, and M. R. Leys, Appl. Phys. Lett. **85**, 4379 (2004).
[5] C. B. Vartuli, S. J. Pearton, C. R. Abernathy, J. D. MacKenzie, E. S. Lambers, and J. C. Zolper, J. Vac. Sci. Technol. B **14**, 3523 (1996).
[6] P. R. Chalker, D. Morrice, T. B. Joyce, T. C. Q. Noakes, P. Bailey, and L. Considine, Diamond Relat. Mater. **9**, 520 (2000).
[7] S.-N. Lee, H. S. Paek, J. K. Son, T. Sakong, Y. N. Kwon, O. H. Nam, and Y. Park, Phys. Status Solidi C **4**, 141 (2007).
[8] N. K. van der Laak, R. A. Oliver, M. J. Kappers, and C. J. Humphreys, J. Appl. Phys. **102**, 013513 (2007).
[9] R. Datta, M. J. Kappers, M. E. Vickers, J. S. Barnard, and C. J. Humphreys, Superlattices Microstruct. **36**, 393 (2004).
[10] R. A. Oliver, M. J. Kappers, J. Sumner, R. Datta, and C. J. Humphreys, J. Cryst. Growth **289**, 506 (2006).
[11] R. Datta, M. J. Kappers, J. S. Barnard, and C. J. Humphreys, Appl. Phys. Lett. **85**, 3411 (2004).
[12] I. Horcas, R. Fernández, J. M. Gómez-Rodríguez, J. Colchero, J. Gómez-Herrero, and A. M. Baro, Rev. Sci. Instrum. **78**, 013705 (2007).
[13] W. M. Tong and R. S. Williams, Annu. Rev. Phys. Chem. **45**, 401 (1994).
[14] D. D. Koleske, M. E. Coltrin, K. C. Cross, C. C. Mitchell, and A. A. Allerman, J. Cryst. Growth **273**, 86 (2004).
[15] R. A. Oliver, M. J. Kappers, and C. J. Humphreys, Phys. Status Solidi C **5**, 1475 (2008).
[16] R. A. Oliver, M. J. Kappers, C. J. Humphreys, and G. A. D. Briggs, J. Appl. Phys. **97**, 013707 (2005).
[17] C. Herring, J. Appl. Phys. **21**, 301 (1950).
[18] J. Neugebauer, Phys. Status Solidi C **0**, 1651 (2003).